

OBSERVATIONS OF LEONID METEORS USING A MID-WAVE INFRARED IMAGING SPECTROGRAPH

G. S. ROSSANO, R.W. RUSSELL, D.K. LYNCH,
T.K. TESSENSOHN, AND D. WARREN

The Aerospace Corporation, M2/266, 2350 E. El Segundo Blvd., El Segundo, CA 90245

E-mail: george.s.rossano@aero.org

and

P. JENNISKENS

SETI Institute, NASA Ames Research Center, Mail Stop 239-4, Moffett Field, CA 94035

E-mail: pjenniskens@mail.arc.nasa.gov

(Received 7 July 2000; Accepted 20 July 2000)

Abstract. We report broadband 3-5.5 μm detections of two Leonid meteors observed during the 1998 Leonid Multi-Instrument Aircraft Campaign. Each meteor was detected at only one position along their trajectory just prior to the point of maximum light emission. We describe the particular aspects of the Aerospace Corp. Mid-wave Infra-Red Imaging Spectrograph (MIRIS) developed for the observation of short duration transient events that impact its ability to detect Leonid meteors. This instrument had its first deployment during the 1998 Leonid MAC. We infer from our observations that the mid-wave IR light curves of two Leonid meteors differed from the visible light curve. At the points of detection, the infrared emission in the MIRIS passband was 25 ± 4 times that at optical wavelengths for both meteors. In addition, we find an upper limit of 800 K for the solid body temperature of the brighter meteor we observed, at the point in the trajectory where we made our mid-wave IR detection.

Keywords: Ablation, Leonids 1998, meteors, meteoroids, mid-IR emission,

1. Introduction

The Aerospace Corporation Mid-wave Infra-Red Imaging Spectrograph (MIRIS) was initially developed as a proof of concept instrument to test the feasibility of producing a mid-wave infrared spectrograph using a binary-optic grism (a transmission grating produced on a shallow angle prism) fabricated using semiconductor etching technology as the dispersing element (Warren *et al.*, 1994; 1998). Having successfully demonstrated the practicality of using such a grism as a dispersing element, MIRIS was developed into an operational instrument which was optimized

for the study of transient events with a time resolution as short as 1 msec, making MIRIS uniquely suited for mid-wave IR observations of meteors. The first fully operational use of MIRIS was to observe the Leonid meteor storm as part of the 1998 Leonid Multi-instrument Airborne Campaign (Jenniskens and Butow, 1999). We describe here the observations made during the intense 1998 Leonid shower in which two broadband detections of Leonid meteors were obtained. As far as we are aware, these detections are the first published mid-wave IR observations of meteors.

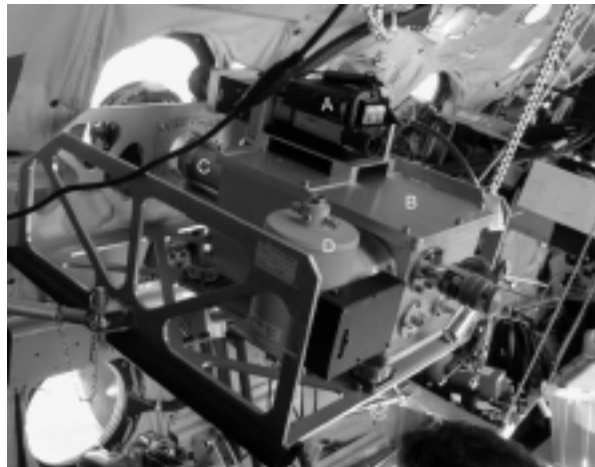


Figure 1. MIRIS installed on FISTA during the Leonid meteor observations. Intensified visible video camera (A) mounted on top provides visible reference images of the field of view. Rectangular vacuum case (B) contains cooled reimaging and dispersing optics. F/15 Objective lens (C) is mounted outside the vacuum case. InSb infrared camera head (D) is mounted on the left side of the case. 228 mm f/15 objective lens at front of case views the sky through an observing port in the aircraft skin.

2. Instrumentation

2.1. INSTRUMENT LAYOUT

MIRIS (Figure 1) consists of three modules: uncooled refractive collecting optics; cooled reimaging optics; and an InSb detector array system (camera head). The camera head and reimaging optics can be cooled independently of each other and the system can be operated with warm reimaging optics for alignment and testing.

The objective lens is made up of two Si elements and one Ge element with an effective focal length of 228 mm and a speed of f/15. All lens

elements in the system are anti reflection coated for the 3.0–5.5 μm band pass of the instrument.

The reimaging optics and grism are located in a rectangular LN_2 dewar and are cooled to an operating temperature of 150 K. This temperature was chosen to reduce the background from the reimaging optics to a manageable level without fully stressing the grism to the extent it would have been by cooling it to 77 K.

The camera lens focal plane lies 1 cm inside the reimaging optics dewar and is illuminated through a 3 in diameter antireflection coated ZnSe window. The reimaging optics reduce the image by a factor of 6 to produce an effective system focal length of 38 mm at the detector focal plane. The objective lens can be removed and other collecting optics (e.g., an astronomical telescope) can be used instead.

The camera head is a modified Amber Model 4256 InSb infrared camera. The final element of the reimaging optics and the system's 3.0–5.5 μm bandpass filter are located within the Amber LN_2 dewar and are cooled to 77 K, as is the detector array. The detector array in the camera head is a 256 by 256 element array with 38 μm pixels.

The optics are configured so both the zero and first orders are imaged onto the detector array. The images are optimized for first order so that the spectrum of a point source will illuminate a single row of the detector array in first order. Residual aberrations in the zero order image produce a point spread function that illuminates four (2 by 2) pixels. The full unvignetted field of view overfills the detector array in both zero and first order. The optics are configured so that the zero order is mainly imaged onto the right hand side of the array and the first order spectrum is mainly dispersed across the array on the left hand side of the array.

In this slitless mode of operation some sources seen in zero order will be dispersed entirely off the left hand side of the array, and some sources in zero order imaged entirely off the right hand side of the array will be dispersed onto the middle of the array. In other words, while for a large portion of the detector the zero order images of sources and their first order spectra are imaged onto the detector array, for some positions only the zero order image falls on the detector while for other positions only the first order spectrum falls on the detector. In slitless mode the unvignetted field of view is a 12 degree diameter circle. This mode of operation was used for the 1998 Leonid meteor observations to maximize the chances of a meteor being observed. The slitless mode of operation is intended for the observation of point sources and line sources. Extended sources can also be observed, but with degraded spectral resolution depending on the width of the source in the dispersion direction. Both the spectral and spatial resolution is limited by the pixel size. For 38 μm pixels, the spectral resolution is 0.025 μm and the spatial resolution is 1 mrad. The measured single pixel system sensitivity using the model 4256 camera head in zero order is 1.1×10^{-14} W for a signal-to-noise of 1 in 1 second.

Observations during the 1998 Leonid meteor storm were made aboard the Flying Infrared Signatures Technology Aircraft (FISTA), a modified KC-135E aircraft, as part of the 1998 Leonid MAC. MIRIS was located on a steerable tray affixed to one of the aircraft's viewing windows (Jenniskens and Butow, 2000). The window material through which the observations were made consisted of a 1 cm thick zinc sulfide plate. The instrument was mounted in such a way that the majority of the meteor trails were oriented roughly perpendicular to the dispersion direction.

2.2. DATA ACQUISITION

Data from the camera controller electronics were acquired using a commercially available frame grabber. The data acquisition software was developed at the Aerospace Corporation. The maximum operating speed of the model 4256 camera is 60 Hz resulting in a data rate of 7.5 MB s^{-1} .

Four data acquisition modes are available: snapshot, continuous, burst, and transient. In the snapshot mode a single frame or single coadded group of frames is recorded under user control. In continuous mode a sequence of individual frames or a sequence of coadded frames is recorded under user control. For very high speed data capture the burst mode allows the capture of 64 MB of data at rates of up to 48 MB per second. User triggered transient events can be captured using the transient mode. A cyclic buffer is used allowing pre- and post-event data buffering. When a transient event occurs the user triggers the capture of a sequence of data frames. The user can select the amount of data (number of frames) before and after the trigger that is recorded.

For the Leonid observations we operated in the continuous mode with the data saved to disk in 3 minute blocks. The detector array was operated at a frame rate of 60 Hz and an integration time of 10 msec or less – depending on the background signal level which varied somewhat during the duration of the flight. Data recording was limited at that time to the use of 2 GB JAZ media and the captured data rate was limited by the speed of the JAZ drive. Sequences of individual frames were recorded at a rate of 16.7 Hz; slightly better than every fourth frame from the detector array.

2.3. CALIBRATION

For radiometric calibration we use two different types of blackbody sources - warm plates and hot cavities. We simulate a point source using a blackbody cavity with pinholes of varying sizes. In addition to providing a radiometric calibration, this source is used for focus and alignment checks, and in one method of wavelength calibration.

Warm plate blackbodies that illuminate the full detector array are used for flat fielding and radiometric calibration. Even though in slitless mode the zero order and first order images overlap for parts of the array, by knowing how each order is mapped onto the array we can radiometrically

calibrate the entire detector array. These plates fill the entire field of view and are typically operated at temperatures of 300–360 K. The Leonid data was radiometrically calibrated using measurements of the warm plates made during each flight.

For guiding and visual comparison an intensified video camera was mounted on top of MIRIS and its output videotaped for the duration of the flight. The relative position of the fields was roughly calibrated by pre-flight observation of distant runway and hanger lights.

The MIRIS data files were time-stamped only once at the beginning of each file, which in retrospect was a poor choice. In examining the data subsequent to the mission it was necessary to get an event time off the video tape and then search the corresponding data file over an appropriate range of frames.

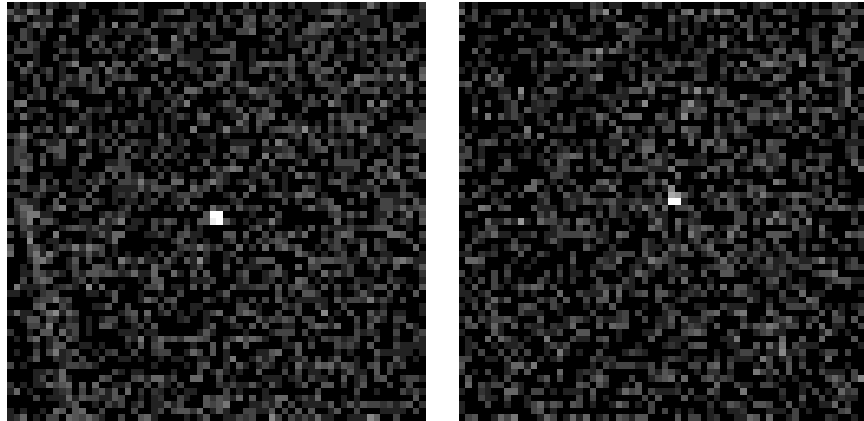


Figure 2. Enlargement of two Leonid meteor detections. Meteor from 17:54:08 UT on the left, and from 20:24:40: UT on the right, Nov. 17, 1998. Scale for each image is 0.064 radians on a side. Intensity is displayed in absolute numbers on a logarithmic scale in order to bring out possible wake. The detections are point sources, with no sign of persisting glow.

3. Results

The three mission video tapes, covering a six hour period, were each examined twice to obtain a record of the time of each meteor seen and an estimate its visible brightness, viz. faint, bright, or very bright. A total of 56 meteors were tabulated that included five very bright meteors including two that occurred while IR data were being recorded. After searching the MIRIS data files for possible detections, we identified one point source at the correct time at 17:54:08 UT. This source was seen in one frame and illuminated four pixels (Figure 2), consistent with the appearance of point sources when observed in zero order by this instrument. An integrated

intensity of $9.0 \times 10^{-12} \text{ W cm}^{-2}$ in the 3.0–5.5 μm bandpass was determined for this meteor. Among the meteors considered bright for which we have examined the data, one other IR detection was made at 20:24:40 UT. This meteor was also only detected in one frame in zero order and illuminated four pixels with an integrated intensity of $5.0 \times 10^{-12} \text{ W cm}^{-2}$ in the 3.0–5.5 μm bandpass (Figure 2). The nominal error for the raw signal counts is 2–3 %. When taking into account the radiometric calibration uncertainty, the total uncertainty in measured brightness is 15%.

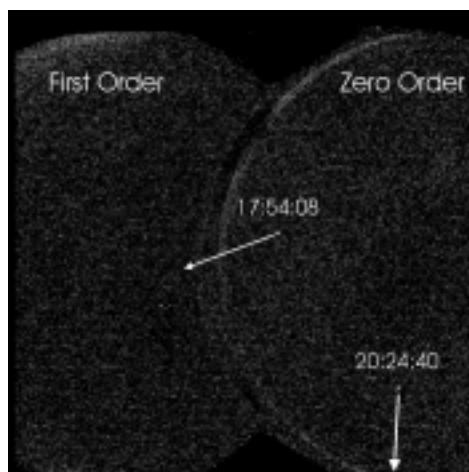


Figure 3. Composite MIRIS image of two Leonid meteor detections at 17:54:08 UT and 20:24:40 UT on a intensity logarithmic scale. By comparing this infrared image to visible images the position of each meteor along its trajectory at the time of the infrared observations was determined. The mid-wave IR detections are the point sources at the ends of the arrows that illustrate the directions of motion determined from the optical images of the meteors. The circular region on the right hand side of the image is the field of view of the instrument in zero order. Infrared radiation is dispersed to the left in first order. The orders overlap in the center of the detector array.

In order to confirm the detections we combined both MIRIS detections into one infrared image (Figure 3) and combined all video frames of the two meteor tracks in one visible image. These two composite images were then overlain adjusting for the different image scales which are both well determined. If the infrared sources are due to meteors then both detections must line up on their corresponding visible tracks in a unique orientation. Such was found to be the case, confirming the detections, determining the points along the trajectories where the infrared detections were made, and allowing a direct comparison of the infrared and visible brightnesses.

Figure 3 shows the composite infrared image and the direction of motion of each meteor determined from the visible trail.

Both meteors were also observed from the accompanying Electra aircraft, which provided multi-station support for stereoscopic measurements (Jenniskens and Butow, 1999). From the FISTA and Electra video records, the trajectories of both meteors were determined with good convergence angles. Both were shown to be Leonid meteors. The different angle of projection on the composite image (Figure 3) is due to different observing directions at the two times.

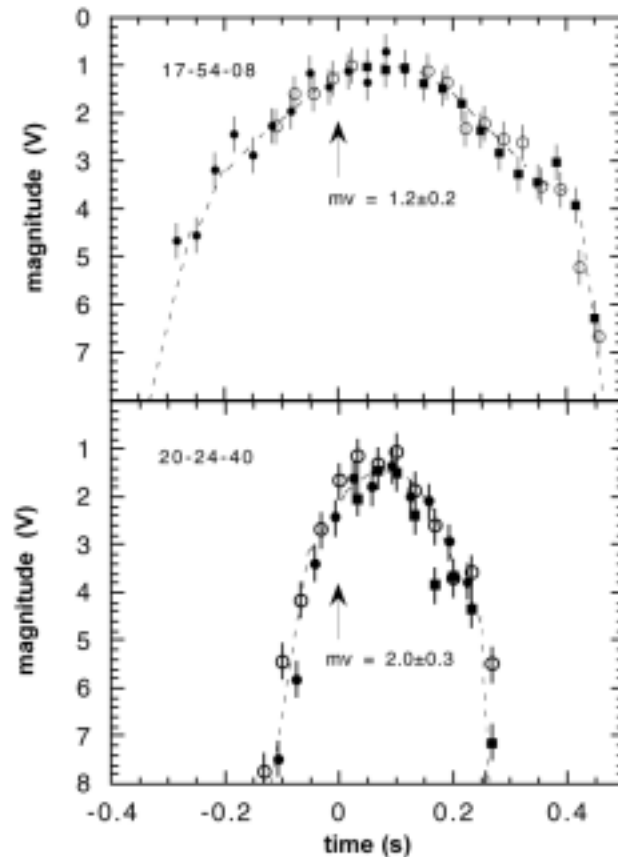


Figure 4. Visible light curves for two Leonid meteors at 17:54:08 UT and 20:24:40 UT detected in the infrared, as determined from visible imagery. Visible magnitude (mv) is plotted versus time, referenced to the time of the infrared observations of each meteor. The magnitude of each meteor at the time of the infrared detections is indicated. The circles, dots and filled squares are the meteor brightnesses measured using three different reference stars in the field of view.

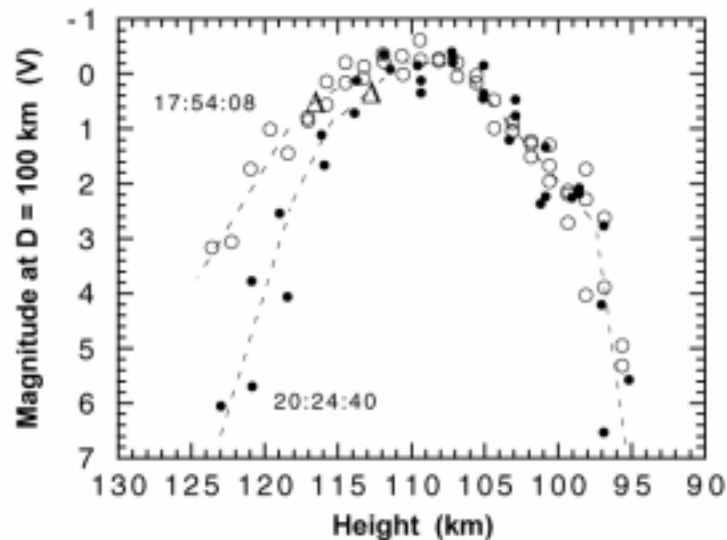


Figure 5. Visual magnitude vs. Height plot for two Leonid mid-IR meteors. Magnitude normalized to a distance of 100 km is plotted vs. height for each meteor. The meteor with the more shallow trajectory (17:54:08 UT) reached a higher brightness early in its trajectory. Below 112 km altitude both meteors were equivalent in absolute brightness vs. altitude. Open circles are the measured visible brightnesses for the 17:54:08 UT meteor while closed circles are for the 20:24:40 UT meteor. The two triangles show the points in the trajectory where the infrared detections were made.

The visible light curves for the two meteors was derived from the video record (Figure 4). The brighter of these two meteors had a visible brightness of $+1.2 \pm 0.2$ magnitude at the time of the IR detection while the fainter meteor had a visible brightness of $+2.0 \pm 0.3$ magnitude. This corresponds to an average $1.24 \pm 0.25 \times 10^{-16} \text{ W cm}^{-2} \text{ \AA}^{-1}$ and $0.59 \pm 0.13 \times 10^{-16} \text{ W cm}^{-2} \text{ \AA}^{-1}$ over the passband of the intensified cameras. The video spectral response is given in Jenniskens (1999), from which we adopt an effective band width of 3161 \AA . Hence, meteors emitted 23 ± 5 and 27 ± 6 times more light in the the MIRIS $3.0\text{--}5.5 \mu\text{m}$ passband than at visible wavelengths at the point of detection.

The meteor that occurred later during the same night at 20:24:40 UT had a shorter trajectory mainly because it entered the atmosphere at a steeper trajectory. Both light curves had a similar shape with a relatively early maximum, a gradual decline that was followed by a rapid decrease of intensity at the end of the trajectory. These light curves resemble those for other Leonid meteors observed on Nov. 17, 1998 as part of the Leonid MAC campaign (Murray *et al.*, 1999). Using the stereoscopic data it is possible to calculate the light curve as a function of altitude (Figure 5).

The light curves are nearly identical below 112 km, but differ early in the trajectory where the more shallow meteor reaches a higher brightness sooner. Surprisingly, the infrared detection of these two meteors were made at a similar altitudes of 117 and 113 km (triangle symbols in Figure 5), just before the maximum in the visible light curve.

4. Discussion

4.1. SINGLE SOURCE DETECTION

The MIRIS frames for both meteors are shown in composite form in Figure 3, with the directions of motion for the two meteors indicated. Given the observed motions of the meteors on the visible videotape (corresponding to approximately 30 infrared pixels of motion per infrared frame), both meteors were still positioned within MIRIS's field of view on the infrared frames following the detection frames, although meteor 17:54:08 UT was only barely so. No hint of detections were seen on either of those frames. For meteor 17:54:08 UT, however, the expected location in the frame subsequent to the detection frame was near the transition from zero to first order where the noise is significantly greater, which may have masked detection in that frame.

If the time development of the infrared light curve followed the trend of the visible light curve then the 20:24:40 UT meteor might have been detected in at least one frame prior to the detection frame, while the 17:54:08 UT meteor might have been detected in at least two frames before being too faint. Tracing back the paths of the two meteors, no detections were seen on any of the preceding frames.

The observations of these meteors in only a single frame, we believe, is partially explained by the high speed motion of the meteors, the low data recording rate, and the particular read out method of the detector array. In the model 4256 camera, integration times shorter than the frame rate are implemented by reducing the number of pixels integrating at any time and progressively scanning across the detector array. For most of our observations the camera was set up with an integration time of about one half the frame time or less, with the meteor trails oriented roughly perpendicular to the detector rows. This means that for most of our observations less than one half the detectors were integrating at any time. In that situation a source moving across rows has a considerable chance of never – or only rarely – illuminating an integrating pixel. However, this is not true for a meteor that moves in a direction generally parallel to the rows, such as meteor 17:54:08 UT.

This results implies that the infrared light curves have faster rise and/or decay times than the visible light curves resulting in a briefer time interval over which meteors are bright enough to be observed in the mid-wave infrared with this instrument – perhaps in the range of 300 msec or less.

If the optical luminosity of meteors is uniform for all meteors with a typical value of 1% the total energy (Jacchia *et al.* 1967), our results imply that about 25% of the emitted intensity is released in the 3.0–5.5 micron passband at the point in the development of the meteors where we made our detection.

4.2. METEOR SPECTRUM

Why did we not detect the first order spectrum of these meteors?

The brighter of the two meteors was observed near the edge of the zero order field of view in the dispersion direction. For that position in the focal plane, the majority of the associated first order spectrum is located off the detector array with only the 3–4 μm wavelength region falling on the array. If the energy detected in zero order were evenly spread out over the 100 pixels that cover a 3–5.5 μm spectrum then a first order spectrum should have been observed at a signal-to-noise ratio of 3. Since we did not detect a signal in the 3–4 μm section of the spectrum we infer that most of the energy observed in zero order lies in the range 4–5.5 μm .

The second meteor we detected was located at a position in the field of view for which the associated first order spectrum was located on the array. For this fainter meteor the anticipated signal-to-noise ratio in first order would have been less than 2 and thus the failure to detect a spectrum is not surprising. Were the energy from these sources primarily in the form of line emission we would have expected a clear first order detection.

For the 4–5.5 μm emission to exceed the 3–4 μm emission, a blackbody temperature of 600 - 700 K is implied. For that temperature range, the IR-to-visible ratio is very much greater than the factor of 25–30 observed. The visible emission of meteors, however, is not due to blackbody emission. Our observations are consistent with the IR emission coming from the ablating meteoroid itself and imply a solid object at a temperature of < 800 K at 115 km altitude but with the visible emission coming from the plasma in the meteor's head and wake.

For at least one of the two meteors we cannot attribute the lack of a detection in the pre-detection frame to the camera timing issue noted above. For the 17:54:08 UT meteor we attribute the lack of a detection in the pre-detection frame to the meteoroid emitting a fainter signal due to a lower meteoroid temperature. Based on the measured noise for the pre-detection frames we derive an upper limit of 450 K for the temperature of this meteoroid 60 msec prior to our detection when the object was at an altitude of 120 km.

5. Conclusions

The two broadband detections reported here are the first published radiometrically calibrated mid-wave infrared detections of meteors. These

detections place constraints on the brightness, spectral characteristics, and time duration of the mid-wave infrared radiation from Leonid meteors. The mid-wave infrared light curve differs from that at optical wavelengths, with significant emission just prior to the peak of the visible light curve, where the luminosity is 25 ± 4 times that at optical wavelengths. From the lack of a first order spectral record in the data, we conclude that the 3.0–5.5 μm emission is primarily a broadband signal with the majority of the emission appearing longward of 4 μm and an upper limit of 800 K for the temperature of the solid body.

The two meteors detected first became visible on the intensified video camera at an altitude of 124 km. At an altitude of 120 km the temperature of at least one of these objects was less than 450 K. By the time the meteoroids reached an altitude of 115 km their temperatures increased to likely values of 600 - 700 K, and were certainly no greater than 800 K. At this point in their trajectories they were still solid objects. Sixty msec later, by which time their visible trails reached maximum brightness, neither meteor was detected in the infrared. We cannot determine if this was due to an actual decrease in the infrared emission from the meteoroids (which one might expect from a decrease in meteoroid surface area as the object ablates), location of the meteoroid signal on detectors where the background noise was higher than elsewhere masking its presence, or instrumental effects related to the detector array timing.

Study of the time development of the infrared signal of similar meteors will require continuous time coverage, preferably at higher frame rates than those used for these observations. The need for such observations was one motivation for the installation of a new Radiance HS camera head added to the system since the 1998 Leonid observations. This new camera head operates in a true snapshot mode, at higher frame rates, and integrates all pixels simultaneously for all integrations times.

Acknowledgments

This work has been supported at the Aerospace Corporation by the Mission-Oriented Investigations and Experiments program, and the Internal Research and Development program. Many Aerospace staff members assisted in making the success of these observations possible. Chief among these were R. Young and M. Ben-Ami who provided key technical support for deployment of the instrument on FISTA. J. Kristl at SDL and his team including T. Hudson, and S. Nierman from Hanscom AFB were generous in providing hardware and technical expertise. U.S. Air Force, MSgt. M. Padilla, Capt. K. Thompson (Edwards AFB) and TSgt. J. Turner (Kadena AFB) offered invaluable critical support. The '98 Leonid MAC was supported by NASA's Exobiology and Planetary Astronomy programs, the NASA Ames Research Center and the NASA

Advanced Missions and Technologies Program for Astrobiology. *Editorial handling*: Frans Rietmeijer.

References

- Jacchia, G.J., Verniani, F., and Briggs, R.E.: 1967, *Smithson. Contrib. Astrophys.* **10**, 1–139.
- Jenniskens, P.: 1999, *Meteoritics Planet. Sci.* **34**, 959–968.
- Jenniskens, P. and Butow, S.J.: 1999, *Meteoritics Planet. Sci.* **34**, 933–943.
- Murray, I.S., Hawkes, R.L., and Jenniskens, P.: 1999, *Meteoritics Planet. Sci.* **34**, 949–958.
- Warren, D.W., Hackwell, J.A., Brames, B.J., and Skinner, W.J.: 1994, in D.L. Crawford (ed.), *Proc. SPIE, vol. 2198, Instrumentation in Astronomy VIII*, [SPIE, Bellingham, WA], pp. 479–486.
- Warren, D.W., Hayhurst, T.L., Rossano, G.S., Hackwell, J.A., and Russell, R.W.: 1998, in A.M. Fowler (ed.), *Proc. SPIE, vol. 3354, Infrared Astronomical Instrumentation*, [SPIE, Bellingham, WA], pp. 168–177.